https://doi.org/10.1093/plphys/kiac251 PLANT PHYSIOLOGY 2022: 190: 113–126

Plant Physiology®

Research Report

Auxin-driven ecophysiological diversification of leaves in domesticated tomato

Juliene d. R. Moreira [1], Bruno L. Rosa [1], Bruno S. Lira [2], Joni E. Lima [3], Ludmila N. F. Correia,[1] Wagner C. Otoni [1], Antonio Figueira [4], Luciano Freschi [2], Tetsu Sakamoto [5], Lázaro E. P. Peres [6], Magdalena Rossi [2] and Agustin Zsögön [1,*,†]

1 Departamento de Biologia Vegetal, Universidade Federal de Viçosa, 36570-900 Viçosa, Minas Gerais, Brazil
2 Departamento de Botânica, Instituto de Biociências, Universidade de São Paulo, 05508-090 São Paulo, Brazil
3 Departamento de Botânica, Instituto de Ciências Biológicas, Universidade Federal de Minas Gerais, 31270-901 Belo Horizonte, Minas Gerais, Brazil
4 Centro de Energia Nuclear na Agricultura, Universidade de São Paulo, 13400-970 Piracicaba, São Paulo, Brazil
5 Bioinformatics Multidisciplinary Environment, Instituto Metrópole Digital, Universidade Federal Do Rio Grande Do Norte, 59078-400 Natal, Rio Grande do Norte, Brazil
6 Laboratory of Hormonal Control of Plant Development, Departamento de Ciências Biológicas (LCB), Escola Superior de Agricultura "Luiz de Queiroz," Universidade de São Paulo, CP 09, 13418-900 Piracicaba, São Paulo, Brazil

*Author for correspondence: agustin.zsogon@ufv.br
†Senior author

J.E.L., L.E.P.P., M.R., and A.Z. conceived the project. J.d.R.M., B.L.R., B.S.L., J.E.L., L.N.F.C., and T.S. performed the experiments. L.F., W.C.O., A.F., L.E.P.P., M.R., and A.Z. supervised the experiments. J.d.R.M. and A.Z. wrote the article with contributions from all the authors. A.Z. agrees to serve as the author responsible for contact.
The author responsible for distribution of materials integral to the findings presented in this article in accordance with the policy described in the Instructions for Authors (https://academic.oup.com/plphys/pages/General-Instructions) is: Agustin Zsögön (agustin.zsogon@ufv.br).

Abstract

Heterobaric leaves have bundle sheath extensions (BSEs) that compartmentalize the parenchyma, whereas homobaric leaves do not. The presence of BSEs affects leaf hydraulics and photosynthetic rate. The tomato (Solanum lycopersicum) obscuravenosa (obv) mutant lacks BSEs. Here, we identify the *obv* gene and the causative mutation, a nonsynonymous amino acid change that disrupts a C2H2 zinc finger motif in a putative transcription factor. This mutation exists as a polymorphism in the natural range of wild tomatoes but has increased in frequency in domesticated tomatoes, suggesting that the latter diversified into heterobaric and homobaric leaf types. The *obv* mutant displays reduced vein density, leaf hydraulic conductance and photosynthetic assimilation rate. We show that these and other pleiotropic effects on plant development, including changes in leaf insertion angle, leaf margin serration, minor vein density, and fruit shape, are controlled by OBV via changes in auxin signaling. Loss of function of the transcriptional regulator AUXIN RESPONSE FACTOR 4 (ARF4) also results in defective BSE development, revealing an additional component of a genetic module controlling aspects of leaf development important for ecological adaptation and subject to breeding selection.

Introduction

Crop domestication was driven by artificial selection to create a loose suite of traits known as the "domestication syndrome" (Hammer, 1984). Considerable effort has been devoted to unveiling the genetic basis of these traits. However, the passage from natural ecosystems to human-managed ones created new drivers for crop evolution that may have had impact beyond the domestication syndrome

Received February 17, 2022. Accepted April 22, 2022. Advance access publication May 27, 2022

(Milla et al., 2015). These drivers include geographic expansion beyond the crops' center of origin, natural selection under cultivation in a highly managed environment, and indirect selection due to constraints caused by developmental trait correlations and physiological trade-offs (Milla et al., 2014). The extent and breadth of the genetic signature created by these processes in crops is not yet known. Understanding the genetic basis of functionally important traits would provide insights for both agricultural and evolutionary studies (Moyle and Muir, 2010). It would further provide valuable support to crop breeding and to the effort of creating new crops using de novo domestication pipelines (Zsögön et al., 2018; Gasparini et al., 2021).

Leaf functional traits are key for resource acquisition and are thus strongly constrained by developmental co-variation (Wright et al., 2004). For instance, high photosynthetic rates require high transpiration capacity, which in turn depends on water transport capacity (Brodribb et al., 2007). Leaf hydraulic conductance is a fundamental driver of leaf diversity, as it is linked with leaf shape, longevity, and venation architecture (Sack and Holbrook, 2006). Notably, many angiosperm species have translucent leaf veins due to the presence of bundle sheath extensions (BSEs), compact columns of chlorophyll-less cells that link the veins to the leaf epidermis (Haberlandt, 1882; Wylie, 1952; Figure 1A). BSEs have considerable functional impact, as they can divide the leaf mesophyll into compartments, resulting in patchy stomatal opening and non-uniform photosynthesis (Terashima, 1992). Leaves harboring such compartments created by BSEs are called heterobaric, as opposed to homobaric ones, where the leaf lamina is topologically continuous (Pieruschka et al., 2010). The effect of BSEs on leaf compartmentalization can be demonstrated by water infiltration in the lamina (Beyschlag and Pfanz, 1990). The presence of BSEs is not restricted to any particular phylogenetic category of plants, but rather appears to be related to functional types in the ecological succession. The distribution of BSEs in natural ecosystems is highly skewed: in a climax forest, most species from the upper strata are heterobaric, whereas those dwelling in the understory are homobaric (Kenzo et al., 2007; Inoue et al., 2015). Likewise, some crops (e.g. soybean—*Glycine max*, sunflower—*Helianthus annuus*) are heterobaric, whereas others (e.g. coffee—*Coffea* spp, cocoa—*Theobroma cacao*, typical understory species in their wild ranges) are homobaric (McClendon, 1992). What determines the distribution of these leaf functional types in natural and agricultural environments? It has been suggested that the presence of BSEs is associated with higher vein densities (Baresch et al., 2019), lower resistance to water flow inside the leaf (Buckley et al., 2015), and higher vessel diameter and transpiration rates (Inoue et al., 2015). However, the lack of a suitable model system to compare heterobaric and homobaric leaf function precludes testing of these hypotheses using a genetic approach. Thus, identifying the genetic basis for BSE development would represent an important steppingstone to unveil BSE function in natural and agricultural settings.

We previously reported that the tomato (*Solanum lycopersicum*) monogenic recessive mutant *obscuravenosa* (*obv*) lacks BSEs in leaves, leading to reduced water transport capacity: both stomatal conductance (g_s) and hydraulic conductance (K_{leaf}) are lower in the mutant compared to wild-type (WT) plants (Zsögön et al., 2015). Here, we identified the *OBV* gene by genetic analysis of introgression lines (ILs) and genome-wide association study (GWAS). We found an increased frequency of the mutation in domesticated tomatoes, and analyzed the geographic distribution of the mutation in the range of tomato wild relatives in South America. Furthermore, we showed that *OBV* alters auxin responses and modulates leaf and fruit shape. Lastly, by analysis of *AUXIN RESPONSE FACTOR 4* (*ARF4*) loss-of-function lines, we found that a genetic module involving auxin response is involved in the development of BSEs. We discuss how this genetic module controlling leaf development and function could be important for ecological adaptation and for breeding selection.

Results

Natural genetic variation for the *obv* mutation in wild tomato species

Analysis of *S. pennellii* ILs in tomato showed that *OBV* locus resides on a chromosome 5 interval defined by the bin d-5E (Figure 1, B and C), which contains 21 genes (Supplemental Table S1; Jones et al., 2007; Chitwood et al., 2013). A GWAS revealed a significant single-nucleotide polymorphism (SNP) in *Solyc05g054030* (Figure 1D and Supplemental Figure S1). The SNP is an A404G nucleotide change in the third exon of the gene coding sequence (CDS), resulting in a predicted histidine to arginine substitution on position 135 (H135R) of the protein (Figure 1E), which is present in different tomato cultivars harboring the *obv* mutation (Supplemental Table S2). Combining genomic and passport information we analyzed the geographic distribution of the mutation in the natural range of tomato wild relatives, including the ancestral species *Solanum pimpinellifolium* (PIM) and the proto-domesticate *S. lycopersicum* var. *cerasiforme* (CER), and found a sympatric cluster of mutant accessions in the lowlands of Ecuador and northern Peru (Figure 1F). Nucleotide diversity analysis on 360 wild and domesticated tomato accessions (available on solgenomics.net) showed that the *OBV* locus resides within a tomato domestication sweep (Figure 1G; Lin et al., 2014). We also found that the mutation increases in frequency between accessions along the wild-domesticated continuum (Figure 1H).

A nonsynonymous SNP is responsible for the *obv* mutation

To test the hypothesis that *Solyc05g054030* encodes the *OBV* gene, we overexpressed (OE) *Solyc05g054030* with (OE^{A404G}) or without (OE^{A404}) the A404G polymorphism in tomato cv. Micro-Tom (MT) homozygous for the *obv* mutation (*obv*/*obv*) (Figure 2A). We observed complementation,

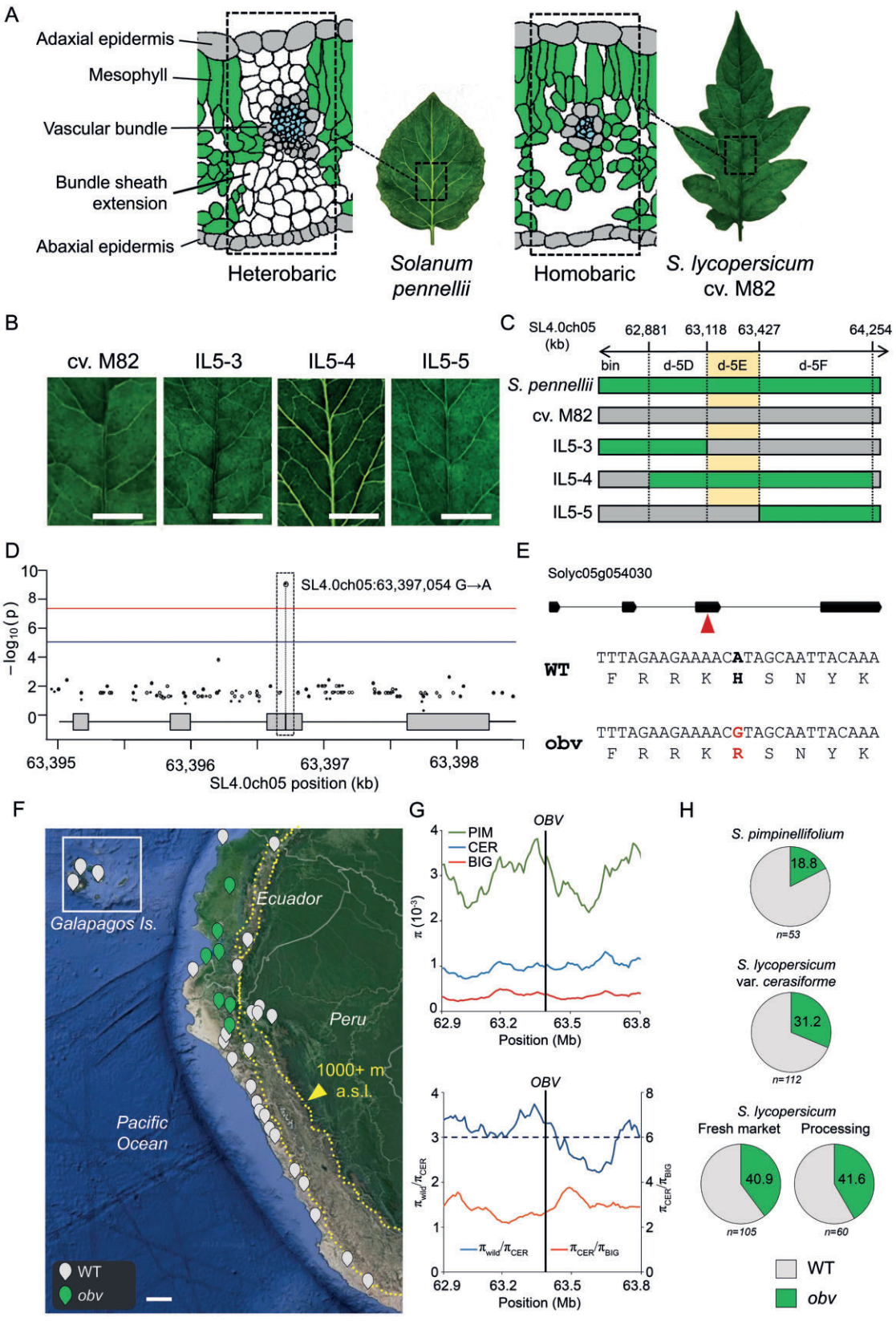

Figure 1 Mapping and identification of a candidate gene for the *obv* mutation. A, Schematic cross-sectional comparison of heterobaric and homobaric leaves. In the heterobaric tomato wild relative *Solanum pennellii* the BSEs are visible as a translucent network of veins, whereas in leaves of tomato (*S. lycopersicum*) harboring the *obv* mutation (such as cv. M82) the leaf lamina appears uniformly green. B, Leaf phenotype of tomato cv. M82 and the *S. pennellii* ILs 5-3, 5-4, and 5-5. Scale bars, 1 cm. C, Bin-mapping of the genomic region containing the *obv* mutation using ILs sequences. D, Association plot of the GWAS for the *obv* phenotype: the *x*-axis represents the chromosome region where Solyc05g054030 is

(continued)

i.e. correct BSE development leading to translucent veins in all *obv* plants harboring the construct lacking the A404G polymorphism (Figure 2B and Supplemental Figure S2), but when the A404G polymorphism was present BSEs were not formed (Figure 2C and Supplemental Figure S3). We further confirmed that the *obv* mutant could be phenocopied by knocking down *Solyc05g054030* expression with an RNA interference (RNAi) construct (Figure 2D). We further crossed two cultivars lacking BSEs (M82 and VFN8) with either the *obv* mutant in the MT background or the *obv* mutant harboring the OBV^{OE} transgene. Hybrid plants derived from the former cross lacked BSEs leading to dark veins, but those derived from the latter showed phenotypic reversion, displaying translucent veins (Figure 2E and Supplemental Figure S4). These results demonstrated that *Solyc05g054030* is *OBV*, the gene responsible for BSE development in tomato leaves, and that a single amino acid change causes the *obv* mutation, which is responsible for the switch from heterobaric to homobaric leaves in tomato. During the preparation of this manuscript the gene identity of *obv* was independently reported and coincides with our own results (Lu et al., 2021).

To better understand the nature of the genetic change underlying the *obv* mutation, we conducted *in silico* analyses of the gene and protein sequences of *OBV* (Figure 2F). The complete sequence of the *OBV* gene encodes a 381-amino acid protein containing three Cys_2-Hys_2 (C2H2) Zn finger domains, which are associated with DNA-binding capability (Persikov et al., 2015), an ethylene-responsive element binding factor-associated amphiphilic repression (EAR) domain, defined by the LxLxL motif and associated with transcriptional repression (Baile et al., 2021), and a carboxy-terminal coiled coil domain, which may function as molecular spacer or macromolecular scaffold (Truebestein and Leonard, 2016). Gene ontology (GO) terms associated with this protein are nucleic acid binding (GO:0003676) and metal ion binding (GO:0046872) (Supplemental Table S3). Using 324 protein sequences of the *OBV* orthologous group from 39 plant species (Emms and Kelly, 2019; Supplemental Table S4) we pinpointed the H135R amino acid change of the *obv* mutant to a highly conserved motif of the second Zn finger domain (Figure 2G). Protein modeling showed that the C2H2 motif is contained within a ββα structure, forming a functional unit internally stabilized by chelation of a single Zn ion (Figure 2F). This suggests that the *obv* mutation leads to complete loss of protein function via disruption of its tertiary structure. Targeted phylogenetic analysis in relevant crop and model species revealed an ancient evolutionary origin of the *OBV* gene with great expansion due to duplication events (Figure 2G and Supplemental Figure S5). Protein sequence alignment of the Zn finger motif that contains the *obv* mutation in tomato showed that even the most phylogenetically distant species have high sequence identity across the domain, suggesting a conserved protein function (Figure 2G). The closest Arabidopsis orthologs of *OBV* (*INDETERMINATE DOMAIN 14*, *15*, and *16*), encode proteins involved in shoot gravitropism and regulation of auxin biosynthesis and transport (Supplemental Table S4 and Supplemental Figure S6; Cui et al., 2013).

BSE development is dependent on auxin signaling

We next characterized the expression profile of *OBV* and found the gene to be highly expressed in meristems, leaf primordia, expanding and mature leaves and flowers (Figure 3, A and B). Altered *OBV* expression levels in the transgenic lines led to changes on leaf insertion angle, leaf margin serration, and fruit shape (Figure 3, C–E), which hinted at a potential role for auxin as a mediator of BSE development. Auxins, like other plant hormones, exert their effect through alterations in metabolism, transport, and sensitivity (Gallei et al., 2020). We found no differences in either auxin content nor in polar auxin transport between WT, the *obv* mutant, and OBV^{OE} lines in leaf primordia (Supplemental Figure S7). However, GUS expression driven by the *DR5* auxin-inducible promoter was increased in the *obv* mutant (Figure 4A) but decreased in the OBV^{OE} lines (Supplemental Figure S8). Exogenous auxin also led to higher inhibition of hypocotyl elongation and stimulation of *in vitro* rhizogenesis from explants in *obv*, compared with WT or OBV^{OE} lines (Supplemental Figure S9). The effects were more obvious in high auxin concentrations than lower ones. This could be at least partially explained by limitations of exogenous hormone treatments, where lower concentrations are more affected by the ability of the tissue to absorb and metabolize the compounds. These results, coupled with the function of the Arabidopsis orthologs of *OBV* as mediators of auxin responses, suggested that *OBV* could be responsible for alterations in auxin signaling. Thus, we next assessed the expression profiles of *AUXIN RESPONSE FACTORS* (*ARFs*) and *AUXIN/INDOLE-3-ACETIC ACID* (*Aux/IAAs*) transcriptional

Figure 1 (Continued)
located, and the *y*-axis represents the negative $\log_{10}$ of *P*-values per SNP derived from the association analysis. The top horizontal line represents the Bonferroni-corrected genome-wide significance threshold ($P = 1.554^{-08}$). The boxes represent the open reading frame of Solyc05g054030. The SNP (an A-to-G transition) located in the third exon of this gene is strongly associated with the *obv* phenotype. E, Gene structure of Solyc05g054030 showing exons (boxes) and introns (lines) and the position of the SNP (arrowhead) in the third exon and DNA and protein sequence of the region around the SNP, showing that it represents a nonsynonymous mutation leading to the substitution of a histidine (H) in the WT for an arginine (R) residue in the *obv* mutant. F, Geographic distribution of accessions of wild tomatoes on the Pacific coast of Peru, Ecuador, and the Galapagos Islands (inset) harboring either the WT or mutant *obv* allele. Scale bar, 100 km. G, Nucleotide diversity (π) of the ancestral wild species *S. pimpinellifolium* (PIM), *S. lycopersicum* var. *cerasiforme* (CER), and big-fruit cultivars (BIG) of domesticated tomato. The horizontal lines indicate genome-wide top 5% cutoff ratio for domestication sweeps. H, Frequency analysis showing the incidence of the *obv* mutation in four different categories of tomato accessions.

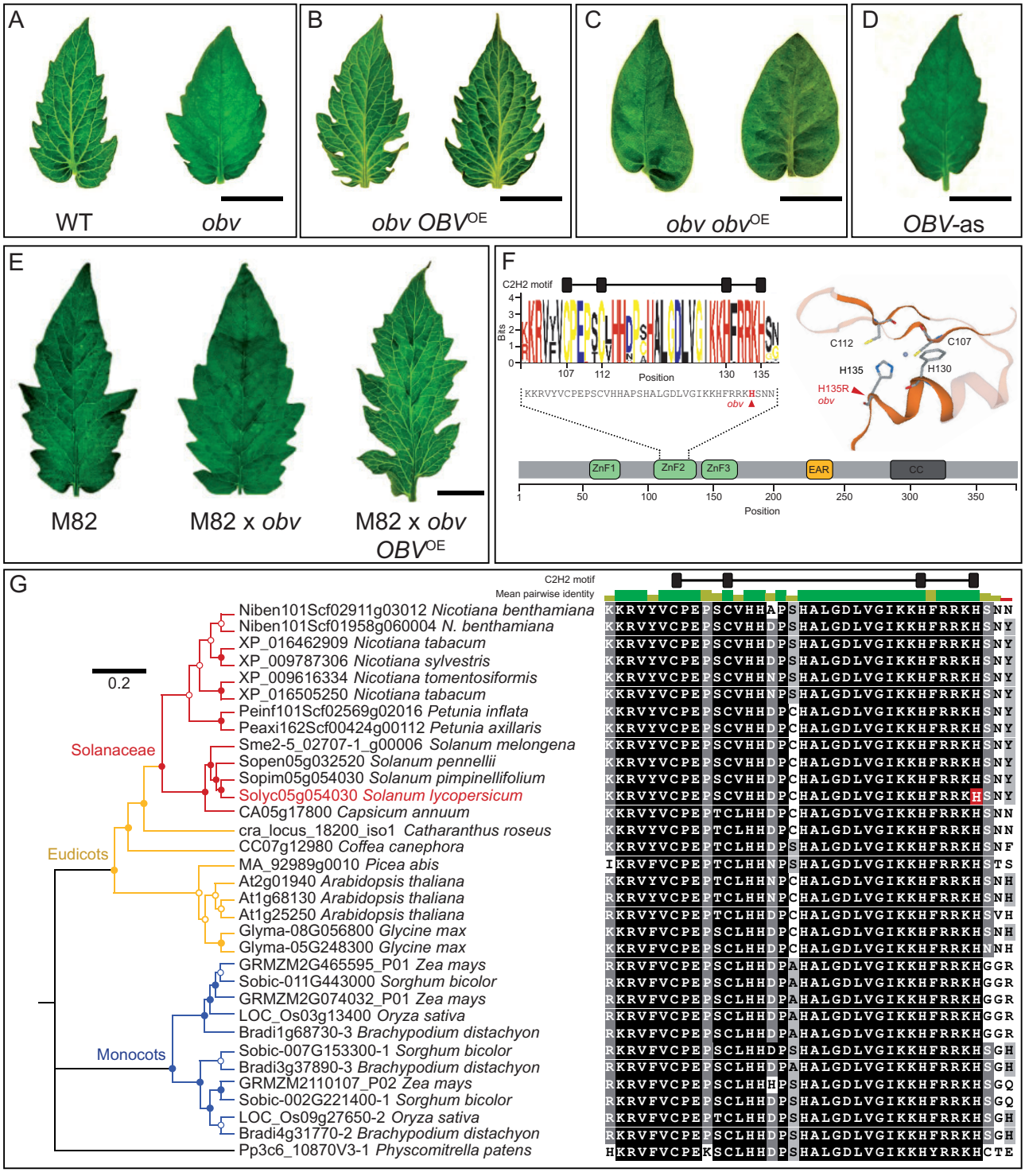

Figure 2 Complementation of the *obv* mutant and protein sequence analysis. A, Representative terminal leaflets of tomato cultivar MT harboring the WT *OBV* allele and the *obv* mutant; B and C, independent transgenic *obv* mutants overexpressing (OE) either (B) the WT *OBV* allele or (C) the mutant *obv* allele, and D, an RNAi knockdown *OBV* line in WT background. E, Representative terminal leaflets of tomato cv. M82 (an *obv* mutant), an F_1 hybrid derived from the cross between M82 and MT-*obv* and an F_1 hybrid of M82 and transgenic MT-*obv* harboring the *OBV* overexpression transgene. Scale bars, 1 cm. F, Schematic representation of the *OBV* protein showing conserved domains: ZnF (zinc finger), EAR (ethylene-responsive EAR), and CC (coiled coil). The sequence of the second ZnF motif (ZnF2) is described as logo plot of residue conservation, with consensus sequence in the bottom. The relative sizes of letters indicate their frequency in an orthologous group of 324 proteins from 39 plant species. The total height of the letters depicts the information content of the position in bits. Right, 3D model of ZnF2 showing the relative positional arrangement of the C_2H_2 residues and the Zn ion ligand. G, Left, maximum-likelihood protein sequence tree of the *OBV* gene in selected model and crop species. Symbols on nodes represent bootstrap support values: full circles >0.75, open circles <0.75. Scale bar, nucleotide substitutions per site. Right, partial protein sequence alignment focused on the second ZnF and showing the histidine (H) residue affected by the *obv*

(continued)

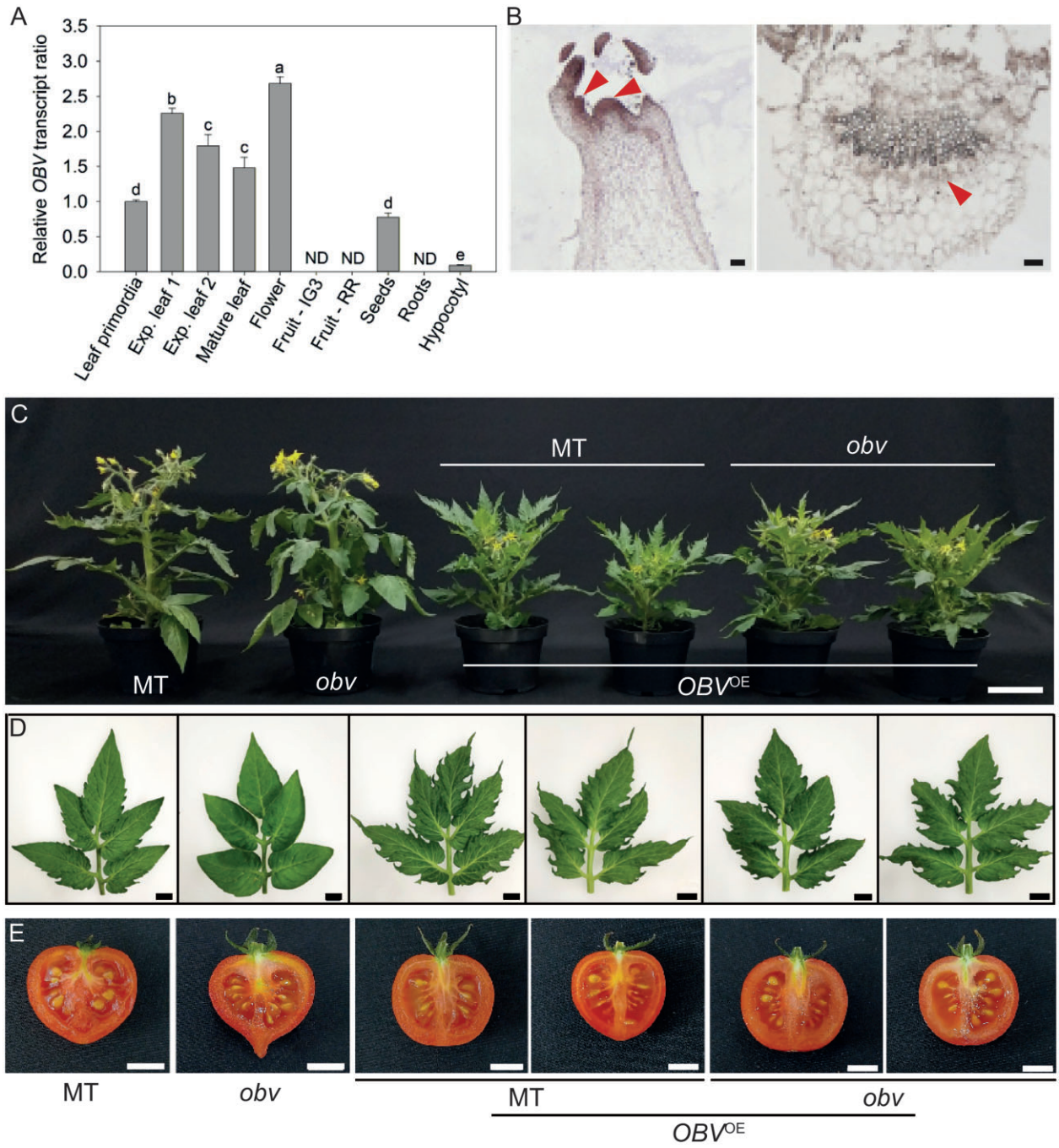

Figure 3 Expression pattern and pleiotropic effects of *OBV* in leaf insertion angle, leaf margin serration, and fruit shape. A, Relative *OBV* mRNA levels in leaves (exp. = expanding), flowers, fruits (ripening stages represented by IG3 = immature green 3 stage fruits; RR = red ripe fruits), seeds, roots, and hypocotyls of tomato cultivar MT. ND = not detected. Data represent mean ± SE ($n = 3$). Different letters indicate statistically significant differences (ANOVA + Tukey's test, $P < 0.05$). B, In situ hybridization showing *OBV* expression patterns in a longitudinal section of the shoot apex, including the apical meristem and leaf primordia and a cross-section of an expanded terminal leaflet. Arrowheads show the specific regions where *OBV* transcripts accumulate. Scale bars, 100 μm. Representative (C) plants, (D) fully expanded fifth leaf, and (E) mature fruits of MT, the *obv* mutant and homozygous T_3 transgenic lines OE the *OBV* gene in either MT or *obv* mutant background. Scale bars, 10 cm (C) and 1 cm (D, E).

Figure 2 (Continued)
mutation in tomato. Shading indicates similarity to consensus (according to Blosum62 score matrix with a threshold of 1): black 100%; dark gray 80%–99%; light gray 60%–79%; white <60%. The bar on the top indicates the mean pairwise identity over all pairs in the column: green 100%; brown 30%–99%, red <30%.

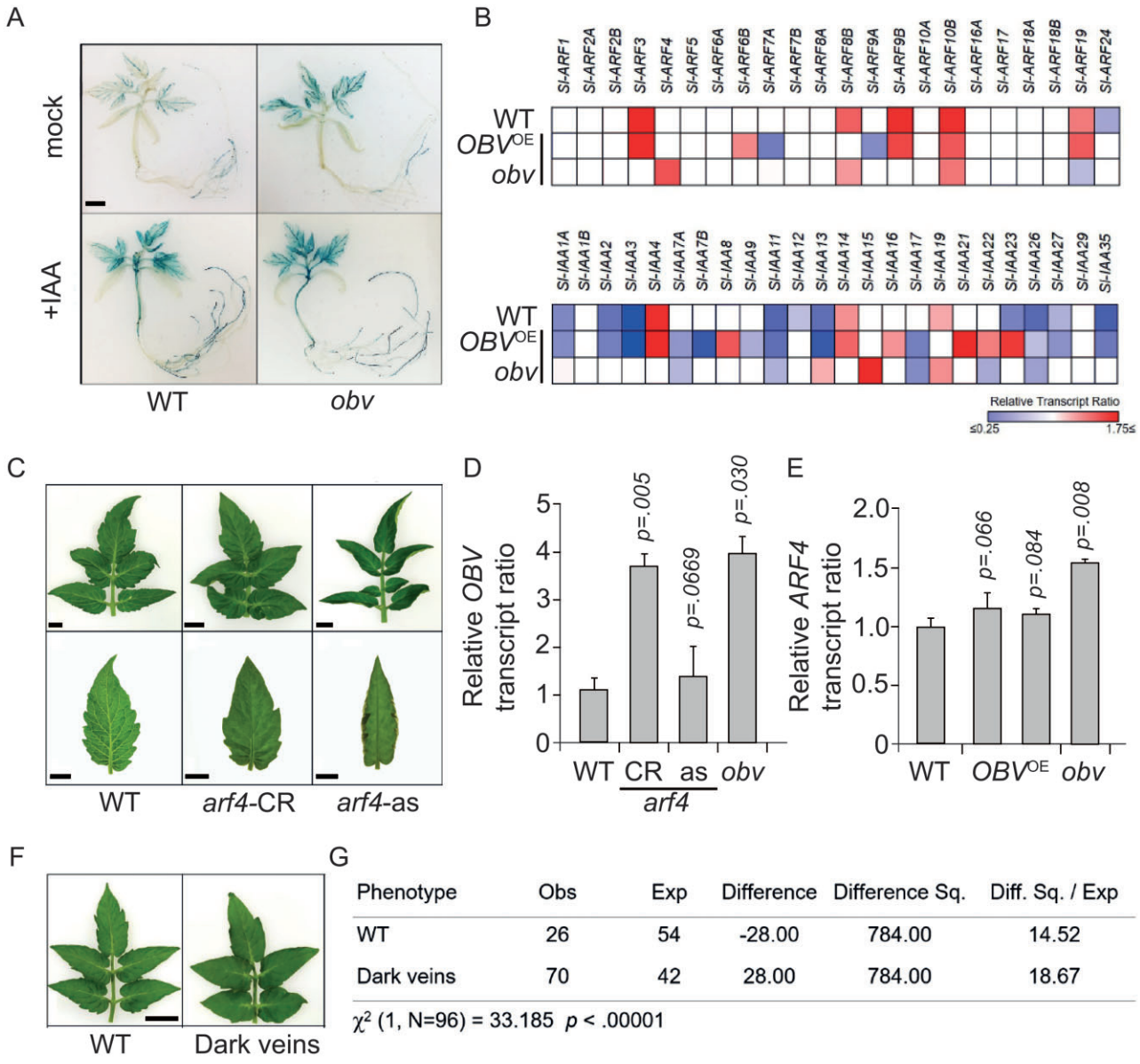

Figure 4 Interaction between *OBV* and auxin signaling in the control of leaf functional type. A, Histochemical GUS analysis in transgenic lines harboring a homozygous *DR5*::*GUS* construct in either WT Micro-Tom or *obv* mutant background. Seedlings were either pre-treated (+ IAA) or not (mock) with 20 μM of indol-3-acetic acid. Scale bar = 1 cm. B, Transcriptional profile of *ARF* and *AUXIN/INDOLE-3-ACETIC* (*Aux/IAA*) genes from leaf primordia. Heat map represents the transcript profiles in two *OBV* OE homozygous transgenic lines (#10 and #12) and the *obv* mutant. Values represent means of four biological replicates normalized against the corresponding WT sample. Statistically significant increases or decreases in comparison with the MT are represented by colored squares ($P < 0.05$). C, Representative leaves and terminal leaflets of MT, a CRISPR *ARF4* mutant (*arf4*-CR) and an antisense *ARF4* knockdown line (*arf4*-as). Scale bars, 1 cm. D, Relative *OBV* mRNA levels in young leaves of MT, *arf4*-CR, *arf4*-as, and *obv*. *P*-values show significant differences to the *obv* mutant. E, Relative *ARF4* mRNA levels in young leaves of MT, homozygous transgenic lines overexpressing (OE) *OBV* and the *obv* mutant. Data represent mean ± SE ($n = 3$). Different letters indicate statistically significant differences (ANOVA + Tukey's test, $P < 0.05$). F–G, Dihybrid analysis for an F_2 population derived from selfing a double heterozygote *OBV obv ARF4 arf4* plant. The goodness of fit analysis was conducted using an expected phenotypic segregation of 9:7, which assumes that both genes act independently.

regulators, which are components of the auxin signal transduction machinery (Truskina et al., 2021). We found consistent upregulation of some *ARFs* (*ARF3*, *9B*, *10B*, *19*, and *AUX/IAA4* and *14*) and downregulation of some *Aux/IAAs* (*Aux/IAA1A*, *1B*, *2*, *3*, *11*, *13*, *26*, and *35*) in OBV^{OE} lines compared with the WT (Figure 4B). In the *obv* mutant, the strongest differences were found for *ARF4* and *Aux/IAA15*, both of which were strongly upregulated compared with the WT (Figure 4B).

Previous work showed that the loss of *ARF4* function has marked effects on leaf development (Sagar et al., 2013; Bouzroud et al., 2020). Thus, we interrogated the potential

role of *ARF4* in BSE development using a CRISPR/Cas9-generated knockout mutant (*arf4*-CR) and a transcriptionally silenced line harboring an *ARF4*-antisense (*ARF4*-as) transgene (Sagar et al., 2013). We found a lack of BSEs and the associated dark vein phenotype in leaves of both *arf4-CR* and *ARF4*-as plants (Figure 4C), which also showed the characteristic inward leaflet curling described previously (Bouzroud et al., 2020). The leaves of both *arf4-CR* and *ARF4*-as plants also showed water infiltration in the lamina and leaf margin serration patterns similar to those of the *obv* mutant (Supplemental Figure S10). Further, *OBV* expression was decreased in *ARF4-as* leaves (Figure 4D) and *ARF4* expression was increased in the *obv* mutant but restored to WT levels in the OBV^{OE} lines (Figure 4E). *In silico* analyses showed that the promoter region of *OBV* contains auxin-response elements (TGTCTC) (Supplemental Figure S11 and Supplemental Table S5), which are typically bound by ARF proteins (Israeli et al., 2020). We conducted a dihybrid analysis to assess potential interaction between OBV and ARF4 by crossing loss-of-function homozygous mutants, selfing the F_1 hybrids and then screening visually a segregating F_2 population. The deviation between expected and observed phenotypic frequencies suggests that gene action between both genes is probably not independent (Figure 4, F–G and Supplemental Figure S12). Taken together, these results suggest that *OBV* controls BSE development *via* interaction with the auxin signaling machinery.

OBV impacts CO_2 assimilation rate and leaf hydraulic conductance

Lastly, we analyzed the functional consequences of allelic variation in *OBV*. We first determined that leaf vein density (vein length per leaf area, VLA) was reduced in *obv* plants (Figure 5, A and B). Vein architecture plays a key role in carbon assimilation rate and water distribution within the leaf (Sack and Scoffoni, 2013). K_{leaf} is a measure of how efficiently water is transported through the leaf: We found that the *obv* mutant had reduced K_{leaf}, which was restored to WT levels in OBV^{OE} transgenic lines (Figure 5C). A regression analysis between VLA and K_{leaf} showed a strong positive correlation ($r = 0.811$, $P < 0.001$) between the variables, with a coefficient of determination (R^2) of 0.657 (Figure 5D). This suggests that variation in VLA caused by *OBV* is a major determinant of variation in K_{leaf}. Interestingly, an auxin biosynthesis mutant with reduced VLA showed reduced K_{leaf} and photosynthetic rate in pea (*Pisum sativum*) (McAdam et al., 2017). Net assimilation of CO_2 (A_n)-chloroplastic CO_2 concentration curves (C_c) (Figure 5E) revealed no difference in maximum Rubisco carboxylation rate (V_{cmax}) (Supplemental Table S6) between genotypes; however, the maximum rate of light-saturated net CO_2 assimilation (A_{max}) was lower in the *obv* mutant (Figure 5F and Supplemental Table S6). This suggests that the presence of BSEs overrides diffusive limitations to photosynthesis through their effect on the water transport capacity of the plants (Buckley et al., 2011; Kawai et al., 2017).

Discussion

Leaf BSEs fulfill important roles in leaf function with large ecophysiological impact. Firstly, by connecting the vascular bundles to the leaf epidermis, BSEs minimize the extra-xylematic path length and favor a greater hydraulic integration in the leaf lamina (Buckley et al., 2011, 2015). The stomata of heterobaric leaves may therefore operate closer to the point of embolism, while responding faster to sudden changes in xylem water potential (Zwieniecki et al., 2007; Inoue et al., 2015). This could at least partially explain the distribution of heterobaric wild tomato accessions in more arid habitats with erratic rainfall patterns (Aybar et al., 2020). Previous work has shown that environmental factors (mainly precipitation regime and intensity of light competition) predict adaptive morphological differentiation between wild tomatoes in their native range (Nakazato et al., 2008, 2010). The most dramatic changes occur in the transition from PIM to CER, which have marked range differences, and include increased leaf area and leaf water content but faster wilting under drought in the latter (Nakazato et al., 2008). Secondly, photosynthetic assimilation rates are higher in heterobaric leaves due to the optimization of light transmission within the leaf lamina (Nikolopoulos et al., 2002). BSEs can function as "transparent windows" that enrich neighboring mesophyll cells (Karabourniotis et al., 2000) or, in the case of C_4 plants, the bundle sheath itself, with high levels of photosynthetically active radiation (400–700 nm) (Bellasio and Lundgren, 2016). The higher photosynthetic assimilation rate in plants harboring the functional *OBV* allele support the contention that heterobaric and homobaric leaves differ in their "carbon-gain strategy" (Liakoura et al., 2009). Lastly, the presence of BSEs increases the plasticity of minor vein density in response to growth light intensity, adjusting water supply and photosynthetic rate to specific environmental conditions (Barbosa et al., 2019). The sum of these effects on leaf function suggests that the presence of BSEs alters the mechanisms that produce the key relations of the leaf economic spectrum (Wright et al., 2004), and is adaptive in local habitats by realizing a trade-off between construction costs and functional gains. This raises the question of what the main driver for the loss of BSEs in domesticated tomato cultivars could be. Since the *obv* mutation increases sensitivity to auxin, we cannot exclude the selection of a favorable pleiotropic effect of this hormone on plant development and productivity (Hu et al., 2018).

The role of auxin in the regulation of leaf morphogenesis and development of vascular tissue is well described (Vanneste and Friml, 2009). Auxin controls leaf margin dissection, which can vary between round/ovate and serrated ("toothed leaves") (Koenig et al., 2009). The loss of *OBV* function leads to rounder leaves, whereas overexpression increases leaf dissection and margin serration. In woody species, increased margin dissection has been associated with colder climates (McKee et al., 2019); however, it is not known if this association is extensive to herbaceous species

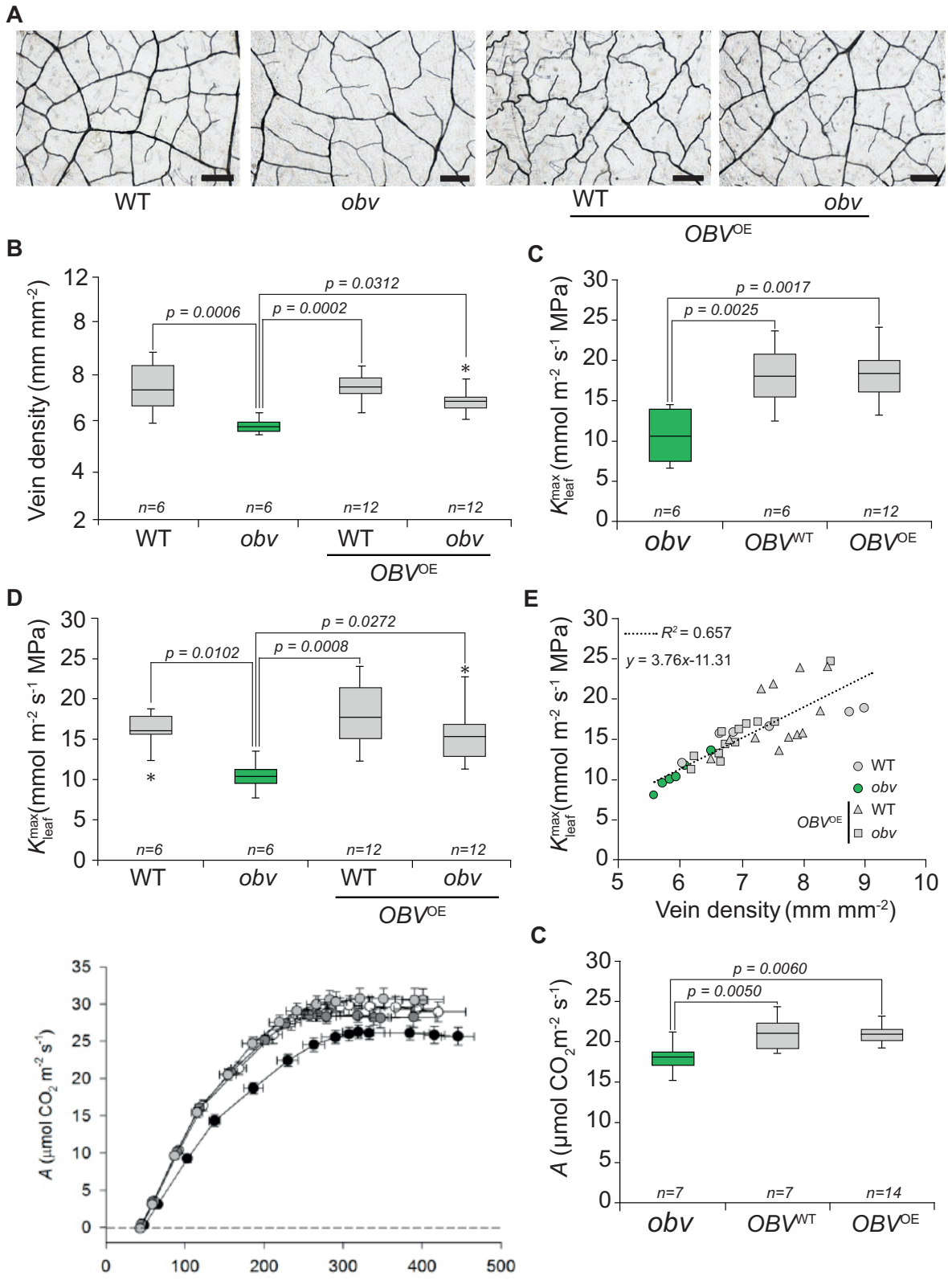

Figure 5 OBV controls vein development and leaf hydraulic conductance (K_{leaf}^{max}) for hydrated leaves. A, Representative micrographs of cleared terminal leaflets of WT tomato cv. MT, the *obv* mutant, and two independent *OBV* OE lines sections in either WT or *obv* background. Scale bars, 100 µm. B, Leaf vein density in WT, *obv*, and the transgenic lines. C, (K_{leaf}^{max}) values in WT, *obv*, and the transgenic lines. D, Regression analysis of (K_{leaf}^{max}) and vein density for WT, *obv*, and the transgenic lines. Each point corresponds to an individual measurement on a different plant. E, Net photosynthetic assimilation (A_n) response curve to CO_2 concentration in the chloroplasts (C_c). F, Maximum assimilation rate at ambient CO_2 and

(continued)

like tomato and its wild relatives. Thus, further analysis of our genotypes could provide insights on the functional relevance of leaf margin serration in annual herbs. Auxin is also a key controller of fleshy fruit development, and plays a role in fruit set upon fertilization and in determination of final fruit size through control of cell division and expansion (Fenn and Giovannoni, 2021). The loss of *ARF4* function leads to a "heart-shaped" fruit (see Figure 2D in Sagar et al., 2013), which is phenocopied by the *obv* mutant. Here, we also showed that *arf4* mutants lack BSEs, which coupled to the reciprocal inhibition of gene expression between *ARF4* and *OBV*, and their epistatic control of BSE development, suggest that they operate together at some level. Future work will address potential physical protein–DNA and protein–protein interactions in these transcription factors. Our results showed that the H135R substitution impairs *OBV* function, and suggest that the amino acid replacement may affect tridimensional protein structure.

The strength of selection against a given amino acid replacement is a function of the chemical similarity between the original amino acid and the nonsynonymous one (Yampolsky et al., 2005). In *obv*, the mutation in position 135 replaces a histidine with an arginine. While both are polar amino acids, histidine is unique with regard to other chemical properties, which means that is does not substitute particularly well with any other amino acid. Our modeling results showed that H135 most likely participates in a metal binding site, acting together with cysteines or other amino acids. It is thus notable that the H135R is not only highly conserved but also found in higher frequency in modern tomato cultivars than in its wild relatives. Homobaric (*i.e.* homozygous *obv* mutants) accessions of the tomato wild relatives are confined to the lowlands of the coastal regions of Ecuador and northern Peru, where a milder, more humid climate prevails (Ilbay-Yupa et al., 2021). These conditions change rapidly going south, due to decreased rainfall, or west, due to increasing altitude in the Andes Mountain range (Moyle, 2008; Aybar et al., 2020). Thus, either purifying selection against the mutation is relaxed under milder conditions, or positive selection favors the homobaric leaf type, selecting against heterobaric leaves' higher construction or operational cost (Read and Stokes, 2006). Interestingly, in wild PIM populations a combination of purifying and balancing selection maintains polymorphism in plant biotic resistance genes (Caicedo, 2008).

When attempting to infer the dynamics of the preservation of a polymorphism in a species three key points ought to be considered: recombination rates (Roselius et al., 2005), mating system (Glémin, 2007), and effective population size (Gaut et al., 2018). Recent work has shown a generally conserved recombination landscape between tomato and its wild relatives (Fuentes et al., 2021). As for mating system, tomato domestication was accompanied by a transition from allogamous wild relatives to autogamous domesticates (Benoit, 2021). Notably, self-fertilization increases the efficiency of purifying selection against slightly deleterious recessive mutations (Byers and Waller, 1999) but aids fixation of favorable recessives (Charlesworth, 1992). Lastly, in species with small effective population size, or that have undergone episodes of strong population bottlenecks, like tomato during its domestication (Razifard et al., 2020, 2021), slightly deleterious mutations can increase in frequency, and eventually even be fixed due to drift (Whitlock, 2000). The strong developmental and functional effects of *OBV*, the skewed geographical distribution of the mutation, and its increasing frequency along the continuum of wild-to-domestic species suggest, however, that genetic drift alone may not be the most satisfactory explanation. An alternative possibility is that the changes in *OBV* allele frequency may have been caused by "genetic hitchhiking", *i.e.* selection on a closely linked locus.

The *OBV* locus resides relatively close (~70 kpb) to *SELF PRUNING 5G* (*SP5G*), a repressor of flowering in long days (Soyk et al., 2017). A hypomorphic allele of this gene was under strong artificial selection during domestication: A severely mitigated long-day induction of *SP5G* caused by a 52-bp deletion explains the near complete loss of daylength-sensitive flowering in domesticated tomato (Zhang et al., 2018; Song et al., 2020). Previous work had suggested that *obv* frequency had increased in processing tomatoes due to selection on *SP5G* for improved growth habit (Jones et al., 2007). It was subsequently shown that *SP5G* is located within a "domestication sweep", revealed by a drastic reduction of nucleotide diversity between PIM and CER (Lin et al., 2014). However, analyzing sequence data from 72 wild and domesticated tomato accessions, we did not find evidence of significant linkage disequilibrium (χ^2 [1, N = 72] = 1.798, P = 0.615) between the *sp5g* and *obv* mutations (Supplemental Tables S7 and S8), suggesting that selection for day neutrality or growth habit (both controlled by *sp5g*) was not a driver of BSE loss through genetic hitchhiking (Barton, 2000). Further, even though sequence variation on chromosome 5 is the main driver of the divergence between fresh and processing tomatoes (Robbins et al., 2011), the incidence of *obv* is very similar in both categories of cultivars. Lastly, a drastic change in the proportion of nonsynonymous mutations occurred during the transition from PIM to CER, and many neutral or beneficial nonsynonymous variants were selected during the northward spread of CER (Razifard et al., 2021). Thus, the population dynamics of the *obv* mutation ought to be considered within this evolutionary

Figure 5 (Continued)
saturating irradiance derived from the curves in (G). Boxes in box plots represent interquartile range (IQR), center line the mean, and the ends of the whisker are set at 1.5*IQR above and below the third and first quartiles, respectively. Asterisks show outliers. *P*-values for significant differences (ANOVA + Tukey's test, $P < 0.05$) are shown.

framework. While it remains an open question whether homobaric leaves are advantageous in an agricultural setting, our results suggest that this may be the case, and the genotypes described here are well-suited to conduct functional analyses of each leaf type under contrasting environments. Analysis of natural genetic variation could also address the ecological contribution of BSEs to adaptation.

Conclusion

Our findings represent an entry point to unravel leaf functional design through a gene-focused approach and provide a molecular anchor for the analysis of phenotypic covariation in leaf anatomical and physiological traits. They also suggest that the divergence in leaf functional types results from a trade-off conditioned by environmental factors and may have adaptive value. The conservation of *OBV* in angiosperms could be leveraged to explore its roles in other plant major crop species and potentially tailor different leaf types to specific agronomic settings. For instance, BSEs were recently shown to provide a pathway for P uptake following foliar fertilization in spring barley (*Hordeum vulgare*) (Arsic et al., 2020). Thus, our discovery of a genetic module controlling the switch between homobaric and heterobaric leaves could have important ecological implications and agricultural applications.

Materials and methods

A full description of all analyses and experiments is available in the Supplemental Materials and Methods.

Plant material, growth conditions, and breeding

Tomato seeds (*S. lycopersicum* cv. Micro-Tom, MT and cv. M82) were sown on polyethylene trays containing Tropostrato commercial substrate (São Paulo, Brazil) and grown in a greenhouse in Viçosa (642 m asl, 20°45′S; 42°51′W), with an average irradiance of ~800 μmol m^{-2} s^{-1}, photoperiod 12-/12-h and air temperature 26/18°C day/night. Upon appearance of the first true leaf, seedlings of MT and M82 were transplanted to pots with a capacity of 350 mL and 3,000 mL, respectively. Soil was fertilized with 2 g L^{-1} NPK (10-10-10) and 4 g L^{-1} limestone. For in vitro cultivation, seeds were sown in flasks containing 30 mL of half-strength MS medium gellified with agar 4 g L^{-1}, pH 5.7 ± 0.05. The seedlings were kept under controlled conditions: photoperiod of 16-h/8-h day/night, light intensity of 45 ± 3 μmol m^{-2} s^{-1}, and temperature of 25 ± 1°C (see Supplemental Materials and Methods for details).

Identification of *OBV* homologs and phylogenetic inference

To identify *OBV* homologs in tomato and other plant species, we retrieved the ortholog group of proteins using the Plant Transcription Factor Database (planttfdb.gao-lab.org) (Supplemental Table S4). We next aligned the sequences from the model species *Arabidopsis thaliana* with MUSCLE (Edgar, 2004). The alignment was submitted to trimAl for alignment trimming (Capella-Gutiérrez et al., 2009) and then submitted to FastTree for tree inference (Price et al., 2010). Trees were visually inspected using FigTree (http://tree.bio.ed.ac.uk/software/figtree/). Further phylogenetic inference using only *OBV* homologs were performed using MUSCLE, for sequence alignment, trimAl, for alignment trimming, SMS, for evolutionary model selection (Lefort et al., 2017), and PHYML, for maximum-likelihood tree inference (Guindon et al., 2010). Final trees were annotated with taxonomic information from NCBI Taxonomy using TaxOnTree (bioinfo.icb.ufmg.br/taxontree). The plant proteomes used in this work were retrieved from Sol Genomics Network (solgenomics.net), for tomato (ITAG v.4.0), and from Uniprot (www.uniprot.org), for other species (see Supplemental Materials and Methods for details).

Gas exchange analyses

Gas exchange analyses were performed in adult plants of cv. M82, M82-*OBV* (cv. M82 harboring the functional *OBV* allele) and M82-OBV^{OE} (M82 plants harboring an *OBV* overexpression construct). All the evaluations described below were measured in terminal leaflets of the fifth expanded leaf. Gas exchange parameters were determined simultaneously using an open-flow infrared gas analyzer system (model LI-6400XT, Li-Cor Inc., Lincoln, Nebraska, USA). The equipment was configured to provide a light intensity of 1,000 μmol m^{-2} s^{-1}, CO_2 concentration of 400 μmol mol^{-1}, with the air flow in the chamber regulated to 300 μmol s^{-1}. The A/C_i response curves were measured under ambient O_2 and temperature, using photosynthetic photon flux density (PPFD) of 1,000 μmol m^{-2} s^{-1} and injection of incremental CO_2 concentrations into the chamber (50, 100, 200, 300, 400, 500, 600, 700, 800, 900, 1,000, 1,200, 1,400, 1,600, and 1,800 μmol mol^{-1}). Calculations of chloroplast concentrations of CO_2 (C_c) and mesophyll conductance (g_m) were performed using the Harley method. The CO_2 compensation point quantified previously for tomato was used as reference to calculate g_m and C_c (see Supplemental Materials and Methods for details).

Statistical analysis

The experimental design was completely randomized. Data were submitted to analysis of variance (ANOVA) and the means were compared by Tukey's test at 5% level of significance ($P \leqslant 0.05$).

Accession numbers

Sequence data from this article can be found in the GenBank/EMBL data libraries under the accession numbers listed in Supplemental Tables S1 and S4.

Supplemental data

The following materials are available in the online version of this article.

Supplemental Figure S1. Mapping and identification of the *OBV* candidate gene.

Supplemental Figure S2. Complementation of the *obv* mutant with the *OBV* functional allele.

Supplemental Figure S3. Complementation of the *obv* mutant and knockdown of the *OBV* gene.

Supplemental Figure S4. Morphology of *OBV*-overexpressing plants in hybrid M82 × MT and VFN8 × MT backgrounds.

Supplemental Figure S5. Maximum-likelihood tree of the OBV family subclade compromising tomato OBV.

Supplemental Figure S6. Phylogenetic reconstruction of the OBV protein family in tomato, Arabidopsis and *Physcomitrium patens*.

Supplemental Figure S7. Influence of OBV on leaf free auxin concentration and polar auxin transport in hypocotyl explants.

Supplemental Figure S8. Reduction of auxin sensitivity in OBV-overexpressing lines revealed by histochemical GUS assays.

Supplemental Figure S9. Hypocotyl elongation and *in vitro* rhizogenesis assays show that OBV alter auxin sensitivity.

Supplemental Figure S10. Control of BSEs development by ARF4 and OBV.

Supplemental Figure S11. *In silico* analysis of the *OBV* (*Solyc05g054030*) promoter region.

Supplemental Figure S12. Phenotypic categories analyzed in a dihybrid cross between *arf4* and *obv* mutants.

Supplemental Table S1. *OBV* candidate genes contained in bin d5-E of the *S. pennellii* ILs.

Supplemental Table S2. *OBV* alleles in different *S. lycopersicum* accession and wild species.

Supplemental Table S3. Enrichment analysis by gene ontology for the *OBV* gene.

Supplemental Table S4. Sequences used for phylogenetic and alignment analyses.

Supplemental Table S5. Functional characterization of *OBV* promoter from *S. lycopersicum* cv Heinz 1706.

Supplemental Table S6. Gas exchange and chlorophyll fluorescence parameters determined in fully expanded leaves of different OBV genotypes in the tomato cv. M82 genetic background.

Supplemental Table S7. Contingency table and goodness of fit calculation for the frequencies of WT (*OBV*, *SP5G*) and mutant (*obv*, *sp5g*) alleles found on chromosome 5 in 72 accessions of *S. lycopersicum*, *S. lycopersicum* var. *cerasiforme*, and *S. pimpinellifolium*.

Supplemental Table S8. Accessions used for the linkage disequilibrium analysis between *OBV* and *SP5G* with their respective genotypes.

Supplemental Table S9. Oligonucleotide DNA sequences for PCR primers used in this study.

Supplemental Materials and Methods.

Acknowledgments

We thank Profs Alisdair Fernie and Ralph Bock (Max-Planck Institute, Germany), Prof José Jiménez-Gómez (INRA Versailles, France), Prof. Andrew J. Thompson (Cranfield University), and Diego S. Reartes for valuable discussions and input on the manuscript. We also gratefully acknowledge the support and contributions of the UFV Plant Physiology Graduate Program.

Funding

This work was supported by the Fundação de Amparo à Pesquisa do Estado de São Paulo (FAPESP), Brazil 2016/01128-9; Fundação de Amparo à Pesquisa do Estado de São Paulo (FAPESP), Brazil 2017/14953-0; Conselho Nacional de Desenvolvimento Científico e Tecnológico (CNPq); Coordenação de Aperfeiçoamento de Pessoal de Nível Superior (CAPES), Brazil, Finance Code 001; and Foundation for Research Assistance of the Minas Gerais State (FAPEMIG), Brazil RED-00053-16.

Conflict of interest statement. None declared.

References

Arsic M, Le Tougaard S, Persson DP, Martens HJ, Doolette CL, Lombi E, Schjoerring JK, Husted S (2020) Bioimaging techniques reveal foliar phosphate uptake pathways and leaf phosphorus status. Plant Physiol **183**: 1472–1483

Aybar C, Fernández C, Huerta A, Lavado W, Vega F, Felipe-Obando O (2020) Construction of a high-resolution gridded rainfall dataset for Peru from 1981 to the present day. Hydrol Sci J **65**: 770–785

Baile F, Merini W, Hidalgo I, Calonje M (2021) EAR domain-containing transcription factors trigger PRC2-mediated chromatin marking in Arabidopsis. Plant Cell **33**: 2701–2715

Barbosa MAM, Chitwood DH, Azevedo AA, Araújo WL, Ribeiro DM, Peres LEP, Martins SCV, Zsögön A (2019) Bundle sheath extensions affect leaf structural and physiological plasticity in response to irradiance. Plant Cell Environ **42**: 1575–1589

Baresch A, Crifò C, Boyce CK (2019) Competition for epidermal space in the evolution of leaves with high physiological rates. New Phytol **221**: 628–639

Barton NH (2000) Genetic hitchhiking. Philos Trans R Soc Lond B Biol Sci **355**: 1553–1562

Bellasio C, Lundgren MR (2016) Anatomical constraints to C4 evolution: light harvesting capacity in the bundle sheath. New Phytol **212**: 485–496

Benoit M (2021) From non-self to self: stepwise mutations in transcription factors promote the transition to self-pollination in tomato. Plant Cell **33**: 3183–3184

Beyschlag W, Pfanz H (1990) A fast method to detect the occurrence of nonhomogeneous distribution of stomatal aperture in heterobaric plant leaves. Oecologia **82**: 52–55

Bouzroud S, Gasparini K, Hu G, Barbosa MAM, Rosa BL, Fahr M, Bendaou N, Bouzayen M, Zsögön A, Smouni A, et al. (2020) Down regulation and loss of auxin response factor 4 function using CRISPR/Cas9 alters plant growth, stomatal function and improves tomato tolerance to salinity and osmotic stress. Genes **11**: 272

Brodribb TJ, Feild TS, Jordan GJ (2007) Leaf maximum photosynthetic rate and venation are linked by hydraulics. Plant Physiol **144**: 1890–1898

Buckley TN, John GP, Scoffoni C, Sack L (2015) How does leaf anatomy influence water transport outside the xylem? Plant Physiol **168**: 1616–1635

Buckley TN, Sack L, Gilbert ME (2011) The role of bundle sheath extensions and life form in stomatal responses to leaf water status. Plant Physiol **156**: 962–973

Byers DL, Waller DM (1999) Do plant populations purge their genetic load? Effects of population size and mating history on inbreeding depression. Annu Rev Ecol Syst **30**: 479–513

Caicedo AL (2008) Geographic diversity cline of R gene homologs in wild populations of *Solanum pimpinellifolium* (Solanaceae). Am J Bot **95**: 393–398

Capella-Gutiérrez S, Silla-Martínez JM, Gabaldón T (2009) trimAl: a tool for automated alignment trimming in large-scale phylogenetic analyses. Bioinformatics **25**: 1972–1973

Charlesworth B (1992) Evolutionary rates in partially self-fertilizing species. Am Naturalist **140**: 126–148

Chitwood DH, Kumar R, Headland LR, Ranjan A, Covington MF, Ichihashi Y, Fulop D, Jiménez-Gómez JM, Peng J, Maloof JN, et al. (2013) A quantitative genetic basis for leaf morphology in a set of precisely defined tomato introgression lines. Plant Cell **25**: 2465–81

Cui D, Zhao J, Jing Y, Fan M, Liu J, Wang Z, Xin W, Hu Y (2013) The Arabidopsis IDD14, IDD15, and IDD16 cooperatively regulate lateral organ morphogenesis and gravitropism by promoting auxin biosynthesis and transport. PLoS Genet **9**: e1003759

Edgar RC (2004) MUSCLE: multiple sequence alignment with high accuracy and high throughput. Nucleic Acids Research **32**: 1792–1797

Emms DM, Kelly S (2019) OrthoFinder: phylogenetic orthology inference for comparative genomics. Genome Biol **20**: 238

Fenn MA, Giovannoni JJ (2021) Phytohormones in fruit development and maturation. Plant J **105**: 446–458

Fuentes RR, de Ridder D, van Dijk ADJ, Peters SA (2021) Domestication shapes recombination patterns in tomato. Mol Biol Evol **39**: msab287

Gallei M, Luschnig C, Friml J (2020) Auxin signalling in growth: Schrödinger's cat out of the bag. Curr Opin Plant Biol **53**: 43–49

Gasparini K, Moreira J dos R, Peres LEP, Zsögön A (2021) De novo domestication of wild species to create crops with increased resilience and nutritional value. Curr Opin Plant Biol **60**: 102006

Gaut BS, Seymour DK, Liu Q, Zhou Y (2018) Demography and its effects on genomic variation in crop domestication. Nat Plants **4**: 512–520

Glémin S (2007) Mating systems and the efficacy of selection at the molecular level. Genetics **177**: 905–916

Guindon S, Dufayard J-F, Lefort V, Anisimova M, Hordijk W, Gascuel O (2010) New algorithms and methods to estimate maximum-likelihood phylogenies: assessing the performance of PhyML 3.0. Syst Biol **59**: 307–321

Haberlandt G (1882) Vergleichende Anatomie des assimilatorischen Gewebesystems des Pflanzens. Jahrb Wiss Bot **13**: 74–188

Hammer K (1984) Das Domestikationssyndrom. Kulturpflanze **32**: 11–34

Hu J, Israeli A, Ori N, Sun T (2018) The interaction between DELLA and ARF/IAA mediates crosstalk between gibberellin and auxin signaling to control fruit initiation in tomato. Plant Cell **30**: 1710–1728

Ilbay-Yupa M, Lavado-Casimiro W, Rau P, Zubieta R, Castillón F (2021) Updating regionalization of precipitation in Ecuador. Theor Appl Climatol **143**: 1513–1528

Inoue Y, Kenzo T, Tanaka-Oda A, Yoneyama A, Ichie T (2015) Leaf water use in heterobaric and homobaric leafed canopy tree species in a Malaysian tropical rain forest. Photosynthetica **53**: 177–186

Israeli A, Reed JW, Ori N (2020) Genetic dissection of the auxin response network. Nat Plants **6**: 1082–1090

Jones CM, Rick CM, Adams D, Jernstedt J, Chetelat RT (2007) Genealogy and fine mapping of *Obscuravenosa*, a gene affecting the distribution of chloroplasts in leaf veins and evidence of selection during breeding of tomatoes (*Lycopersicon esculentum*; Solanaceae). Am J Bot **94**: 935–947

Karabourniotis G, Bornman JF, Nikolopoulos D (2000) A possible optical role of the bundle sheath extensions of the heterobaric leaves of *Vitis vinifera* and *Quercus coccifera*. Plant Cell Environ **23**: 423–430

Kawai K, Miyoshi R, Okada N (2017) Bundle sheath extensions are linked to water relations but not to mechanical and structural properties of leaves. Trees **31**: 1–11

Kenzo T, Ichie T, Watanabe Y, Hiromi T (2007) Ecological distribution of homobaric and heterobaric leaves in tree species of Malaysian lowland tropical rainforest. Am J Bot **94**: 764–775

Koenig D, Bayer E, Kang J, Kuhlemeier C, Sinha N (2009) Auxin patterns *Solanum lycopersicum* leaf morphogenesis. Development **136**: 2997–3006

Lefort V, Longueville J-E, Gascuel O (2017) SMS: smart model selection in PhyML. Mol Biol Evol **34**: 2422–2424

Liakoura V, Fotelli MN, Rennenberg H, Karabourniotis G (2009) Should structure–function relations be considered separately for homobaric vs. heterobaric leaves? Am J Bot **96**: 612–619

Lin T, Zhu G, Zhang J, Xu X, Yu Q, Zheng Z, Zhang Z, Lun Y, Li S, Wang X, et al. (2014) Genomic analyses provide insights into the history of tomato breeding. Nat Genet **46**: 1220–1226

Lu J, Pan C, Li X, Huang Z, Shu J, Wang X, Lu X, Pan F, Hu J, Zhang H, et al. (2021) C_2H_2 zinc finger transcription factor, positively regulates chloroplast development and bundle sheath extension formation in tomato (Solanum lycopersicum) leaf veins. Hortic Res **8**: 1–14

McAdam SAM, Eléouët MP, Best M, Brodribb TJ, Murphy MC, Cook SD, Dalmais M, Dimitriou T, Gélinas-Marion A, Gill WM, et al. (2017) Linking auxin with photosynthetic rate via leaf venation. Plant Physiol **175**: 351–360

McClendon JH (1992) Photographic survey of the occurrence of bundle-sheath extensions in deciduous dicots. Plant Physiol **99**: 1677–1679

McKee ML, Royer DL, Poulos HM (2019) Experimental evidence for species-dependent responses in leaf shape to temperature: implications for paleoclimate inference. PLoS ONE **14**: e0218884

Milla R, Morente-López J, Alonso-Rodrigo JM, Martín-Robles N, Chapin FS (2014) Shifts and disruptions in resource-use trait syndromes during the evolution of herbaceous crops. Proc R Soc B **281**: 20141429–20141429

Milla R, Osborne CP, Turcotte MM, Violle C (2015) Plant domestication through an ecological lens. Trends Ecol Evol **30**: 463–469

Moyle LC (2008) Ecological and evolutionary genomics in the wild tomatoes (solanum Sect. Lycopersicon). Evolution **62**: 2995–3013

Moyle LC, Muir CD (2010) Reciprocal insights into adaptation from agricultural and evolutionary studies in tomato. Evol Appl **3**: 409–421

Nakazato T, Bogonovich M, Moyle LC (2008) Environmental factors predict adaptive phenotypic differentiation within and between two wild Andean tomatoes. Evolution **62**: 774–792

Nakazato T, Warren DL, Moyle LC (2010) Ecological and geographic modes of species divergence in wild tomatoes. Am J Bot **97**: 680–693

Nikolopoulos D, Liakopoulos G, Drossopoulos I, Karabourniotis G (2002) The relationship between anatomy and photosynthetic performance of heterobaric leaves. Plant Physiol **129**: 235–243

Persikov AV, Wetzel JL, Rowland EF, Oakes BL, Xu DJ, Singh M, Noyes MB (2015) A systematic survey of the Cys2His2 zinc finger DNA-binding landscape. Nucleic Acids Res **43**: 1965–1984

Pieruschka R, Chavarría-Krauser A, Schurr U, Jahnke S (2010) Photosynthesis in lightfleck areas of homobaric and heterobaric leaves. J Exp Bot **61**: 1031–1039

Price MN, Dehal PS, Arkin AP (2010) FastTree 2—approximately maximum-likelihood trees for large alignments. PLoS ONE **5**: e9490

Razifard H, Ramos A, Della Valle AL, Bodary C, Goetz E, Manser EJ, Li X, Zhang L, Visa S, Tieman D, et al. (2020) Genomic evidence for complex domestication history of the cultivated tomato in Latin America. Mol Biol Evol **37**: 1118–1132

Razifard H, Visa S, Tieman D, van der Knaap E, Caicedo AL (2021) The Evolutionary Dynamics of Genetic Mutational Load

Throughout Tomato Domestication History. Cold Spring Harbor Laboratory. Doi:2021.11.08.467620

Read J, Stokes A (2006) Plant biomechanics in an ecological context. Am J Bot **93**: 1546–1565

Robbins MD, Sim S-C, Yang W, Van Deynze A, van der Knaap E, Joobeur T, Francis DM (2011) Mapping and linkage disequilibrium analysis with a genome-wide collection of SNPs that detect polymorphism in cultivated tomato. J Exp Bot **62**: 1831–1845

Roselius K, Stephan W, Städler T (2005) The relationship of nucleotide polymorphism, recombination rate and selection in wild tomato species. Genetics **171**: 753–763

Sack L, Holbrook NM (2006) Leaf hydraulics. Annu Rev Plant Biol **57**: 361–381

Sack L, Scoffoni C (2013) Leaf venation: structure, function, development, evolution, ecology and applications in the past, present and future. New Phytol **198**: 983–1000

Sagar M, Chervin C, Mila I, Hao Y, Roustan J-P, Benichou M, Gibon Y, Biais B, Maury P, Latché A, et al. (2013) SlARF4, an auxin response factor involved in the control of sugar metabolism during tomato fruit development. Plant Physiol **161**: 1362–1374

Song J, Zhang S, Wang X, Sun S, Liu Z, Wang K, Wan H, Zhou G, Li R, Yu H (2020) Variations in both FTL1 and SP5G, two tomato FT paralogs, control day-neutral flowering. Mol Plant **13**: 939–942

Soyk S, Müller NA, Park SJ, Schmalenbach I, Jiang K, Hayama R, Zhang L, Van Eck J, Jimenez-Gomez JM, Lippman ZB (2017) Variation in the flowering gene SELF PRUNING 5G promotes day-neutrality and early yield in tomato. Nat Genet **49**: 162–168

Terashima I (1992) Anatomy of nonuniform leaf photosynthesis. Photosynth Res **31**: 195–212

Truebestein L, Leonard TA (2016) Coiled-coils: the long and short of it. Bioessays **38**: 903

Truskina J, Han J, Chrysanthou E, Galvan-Ampudia CS, Lainé S, Brunoud G, Macé J, Bellows S, Legrand J, Bågman A-M, et al. (2021) A network of transcriptional repressors modulates auxin responses. Nature **589**: 116–119

Vanneste S, Friml J (2009) Auxin: A Trigger for Change in Plant Development. Cell **136**: 1005–1016

Whitlock MC (2000) Fixation of new alleles and the extinction of small populations: drift load, beneficial alleles, and sexual selection. Evolution **54**: 1855–1861

Wright IJ, Reich PB, Westoby M, Ackerly DD, Baruch Z, Bongers F, Cavender-Bares J, Chapin T, Cornelissen JHC, Diemer M, et al. (2004) The worldwide leaf economics spectrum. Nature **428**: 821–827

Wylie RB (1952) The bundle sheath extension in leaves of dicotyledons. Am J Bot **39**: 645–651

Yampolsky LY, Kondrashov FA, Kondrashov AS (2005) Distribution of the strength of selection against amino acid replacements in human proteins. Hum Mol Genet **14**: 3191–3201

Zhang S, Jiao Z, Liu L, Wang K, Zhong D, Li S, Zhao T, Xu X, Cui X (2018) Enhancer–promoter interaction of SELF PRUNING 5G shapes photoperiod adaptation. Plant Physiol **178**: 1631–1642

Zsögön A, Alves Negrini AC, Peres LEP, Nguyen HT, Ball MC (2015) A mutation that eliminates bundle sheath extensions reduces leaf hydraulic conductance, stomatal conductance and assimilation rates in tomato (*Solanum lycopersicum*). New Phytol **205**: 618–626

Zsögön A, Čermák T, Naves ER, Notini MM, Edel KH, Weinl S, Freschi L, Voytas DF, Kudla J, Peres LEP (2018) De novo domestication of wild tomato using genome editing. Nat Biotechnol **36**: 1211–1216

Zwieniecki MA, Brodribb TJ, Holbrook NM (2007) Hydraulic design of leaves: insights from rehydration kinetics. Plant Cell Environ **30**: 910–921